Hindawi
Advances in Materials Science and Engineering
Volume 2023, Article ID 8539809, 10 pages
https://doi.org/10.1155/2023/8539809

Research Article

Analysis of Maximizing the Power Output of Switched Reluctance Generator Using Different Core Materials

M. Ramkumar and K. Latha

Department of Electrical and Electronics Engineering, College of Engineering Guindy, Anna University, Chennai 600025, India

Correspondence should be addressed to M. Ramkumar; m.ramkumarphd@gmail.com

Received 5 December 2022; Revised 3 January 2023; Accepted 4 January 2023; Published 16 January 2023

Academic Editor: Dimitrios E. Manolakos

Switched reluctance generator (SRG) has become the key focus of research for its usage in wind power generation. The sizing and performance of SRG depend on the core material used for the stator and rotor. This paper analyses the impact of the magnetic loading of different core materials on the performance of SRG in terms of self-inductance, torque, iron losses, ohmic losses, and generated voltage. 1 kW SRG with different pole configuration 8/6 SRG and 12/8 SRG for the wind speed of 3 m/s to 6 m/s has been designed. Static and dynamic analyses using the finite element analysis (FEA) were carried out for analytically designed 1 kW SRG with different core materials with the same lamination thickness. Prototypes of 8/6 SRG and 12/8 SRG are fabricated. The output of simulation results has been validated by experimental measurements.

1. Introduction

Recently, due to environmental problems, there is an increased usage of natural resources for power generation. Wind energy is a natural source and to generate electricity at a variable speed, a generator and converter are needed. Doubly-fed induction generators (DFIGs), induction generators (IGs), and permanent magnet synchronous generators (PMSGs) have been used for wind power generator systems (WPGSs). Recently the potential development of SRG for small-size WPGS has gained popularity. Switched reluctance generator (SRG) has a simple structure without any brushes, winding, or permanent magnets in the rotor. SRG has lower cost, high power generation efficiency, small inertia, lower startup torque, excellent lower speed performance, and a wide variable speed range. These characteristics make SRG a promising solution for wind power generation systems [1–3].

SRG has to be designed to maximize the power output with reduced losses. The sizing and performance of SRG apart from design methodology also depend on the core material used for the stator and rotor. Choosing a core material for an electrical machine for an application depends upon its magnetic properties, mechanical properties, loss characteristics, and cost. One material is not suitable for all applications and there will be a tradeoff between the different properties [4].

The power output of SRG depends on electrical loading and magnetic loading. By increasing the magnetic loading of the core material, the electrical loading will be reduced for the same power output, hence power density is increased. The thermal behavior of the machine depends on the heat developed. The heat sources, which raise the temperature of the components, are core losses and ohmic losses. Ohmic losses depend on electrical loading, and core losses depend on the loss characteristics of the core material. By proper choice of the core material with high strength, high saturation magnetization, and low loss characteristics, we can develop SRG with optimal weight, increased power density, higher efficiency with reduced losses, and good thermal behavior [5].

The stator and rotor are made of thin surface insulated laminations stacked together on an axis. Grain-oriented steel is not suitable for SRG as the flux is not flowing always in one direction. Hence, nongrain-oriented steel is used as core materials. Investigations on the effect of lamination

thickness show that the core losses will increase as the lamination thickness increases. By making the laminations thin the core losses will decrease but will in turn require more laminations leading to higher costs. Stresses are induced when handling thin lamination core materials, which in turn leads to a reduction of magnetic properties [6, 7].

In this paper, the effect of the core material characteristics on the inductance, core loss, ohmic loss, torque, and generated voltage of the SRG has been analyzed and presented.

2. Magnetic Core Materials

The sizing and performance of SRG vary due to the variation in relative permeability and operating flux density for various core materials. The useful ferromagnetic elements for core material are iron, nickel, and cobalt, A few of the rare-earth elements also show ferromagnetic behavior but they are not suitable for the fabrication of a core. The magnetic or mechanical properties vary with the composition of the alloys. The most widely used alloys are low-carbon steel, silicon steel, nickel-iron, and cobalt-iron alloys [8].

Low-carbon steel has low cost and good mechanical properties. Hence, it is used for many applications even though this steel has a high core loss. If low-carbon steel is alloyed with silicon (silicon steel), the resistivity of the material increases which reduces eddy current losses, and a high magnetic flux is achieved as the hysteresis loop is narrowed. Silicon steel is often used in electrical machines as the efficiency is increased. The disadvantage of silicon steel is, that at higher temperatures, this material is susceptible to increased corrosion and oxidation.

Nickel iron alloy, on the other hand, has the highest permeability at the lowest field strength and the lowest core losses. Nickel alloys have a lower saturation level compared to other alloys, which makes them unsuitable for applications where flux density is of prime importance. Nickel iron alloy has a low Curie temperature. The magnetic sensitivity of Nickel iron alloy is the highest compared to all alloys [8–14].

Cobalt iron alloy has the highest flux density, very high permeability, good mechanical strength, and the highest Curie temperature. Due to the high saturation magnetization level, the power density is higher compared to other alloys. Studies have proved that moving from silicon alloy to cobalt iron alloy leads to material reduction of 25% and hence less weight. Cobalt iron alloy is more expensive compared to other alloys [8–14].

In this study, ten different magnetic core steel with 0.35 mm thickness grades shown in Table 1 are considered to analyze the impact of these materials on SRG performance namely generated voltage, iron loss, ohmic loss, and torque for the wind energy standalone systems.

Figure 1 shows the magnetization characteristics (B-H curve) of the materials given in Table 1. The steel Hiperco and HyMu have the highest and lowest relative permeability, respectively until entering the saturation region. Hiperco has a flux density (B) of more than 2 Tesla (T) for magnetic fields (H) greater than 210 A/m, whereas other materials with H greater than 30000 A/m have a flux density of more than 2 T. The flux density (B) of HyMu is less than 1 Tesla (T).

Table 1: Material classifications.

S. no	Material	Type
I	CR steel	Steel
II	Hiperco	Cobalt iron alloy
III	HyMu	Nickel iron alloy
IV	35C240	(IV–VII) nonoriented silicon steel
V	35C300	
VI	35C360	
VII	35C530	
VIII	35C270	Nonoriented fully processed silicon steel material
IX	35C330	
X	Vacoflux	Vacuum schmelze steel materials (cobalt iron alloy)

Figure 2 shows the variation of relative permeability with respect to flux density for the materials chosen. From the figure, it is observed that the permeability of these steels will begin to decrease as the operational flux density increases, due to saturation. HyMu has a high relative permeability of around 400000 and 35C530 has a lower relative permeability of around 7500.

3. Sizing of SRG Using Different Core Materials

The switched reluctance machine can operate both in motoring and generating mode by appropriately energizing the stator phases, during the appropriate instants of inductances with respect to the rotor position [15].

The design of SRG depends on the required electrical power output, phase current, output voltage, and speed.

The number of turns per phase (T_{ph}) is calculated [16] by

$$\lambda_{\text{peak}} = \frac{V_g \varepsilon}{\omega}, \tag{1}$$

$$\omega = \frac{2\pi N}{60}, \tag{2}$$

$$\lambda_{\text{peak}} = 2\, B_m W_s L_{\text{stk}}\, T_{\text{ph}}, \tag{3}$$

$$T_{\text{ph}} = \frac{15\, V_g\, \varepsilon}{N\, \pi\, B_m W_s L_{\text{stk}}}, \tag{4}$$

where λ_{peak} is the peak flux linkage, V_g is the generating voltage, ε is the step angle, N is the generator rotational speed, W_s is the width of the stator, L_{stk} is the stack length, and B_m is the flux density.

The impact of the change of core material can be analyzed in two different ways.

(i) In the first case, keeping the power output constant, the generator can be redesigned for different operating flux densities B_m using different core materials. From equations (1)–(4), keeping V_g generating voltage constant while increasing the flux density stack length, width of the stator, and turns per phase

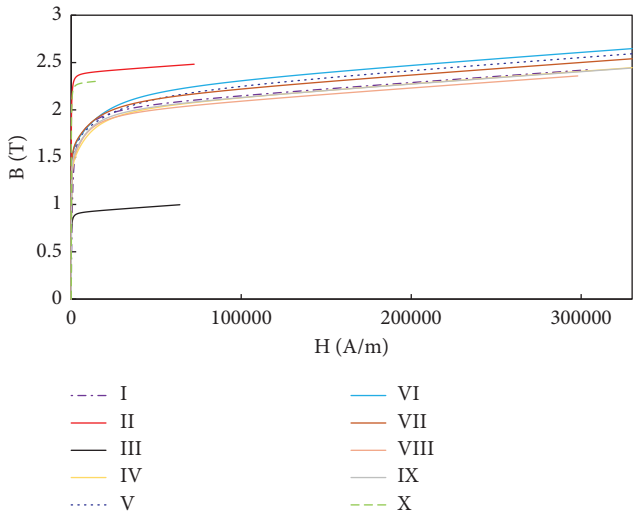

Figure 1: Magnetization curves of magnetic core steels.

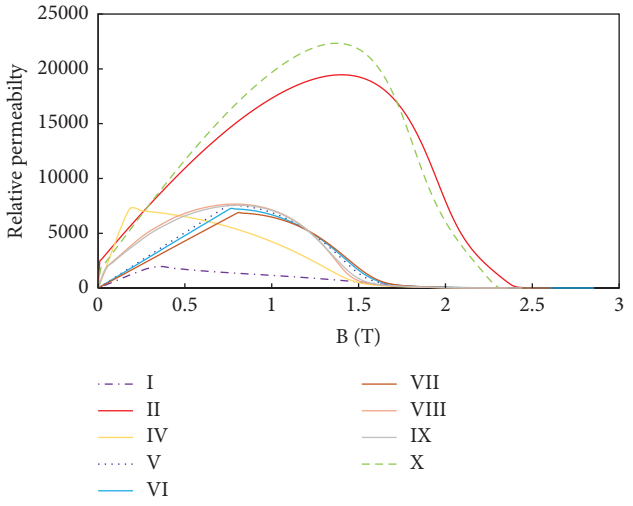

Figure 2: Relative permeability of magnetic core steels.

can be reduced. Based on material flux density, the modified ratio of axial length to rotor diameter (L/D_r) is shown in Table 2 with the power output constant.

From Table 2 it is observed that for higher flux density (B_m) the dimensions of SRG can be decreased and hence the power density is increased. For example, comparing 35C270 (1.8 T) and Hiperco (2.4 T) there is a 24% reduction in material and hence weight is reduced. For an increase in flux density (B_m), the length of the airgap can be increased without changing the dimensions of SRG for the constant power output of SRG. For less air gap, the power output will be better for all core materials. In this paper, an air gap of 0.35 mm is considered.

(ii) In the second case, keeping the dimensions constant the performance of SRG is compared for different flux densities (B_m) using different core materials.

From equations (1)–(4), keeping the width of the stator (W_s), stack length (L_{stk}), and the number of turns per phase (T_{ph}) constant, V_g increases as B_m increases hence power output increases.

The torque (T_e) equation of SRG is given by

$$T_e = \frac{1}{2} i^2 \frac{\partial L}{\partial \theta}, \tag{5}$$

where i is the excitation current.

The variation of inductance (∂L) depends on the aligned inductance and unaligned inductance. Maximizing this variation can increase the torque in the SRG. The aligned inductance depends on the operating flux density of the core material.

In this paper, a detailed study has been carried out on how the inductance, torque, losses, and generated voltage vary based on the core material used keeping the dimensions constant.

4. Core Loss for Different Core Materials

Power loss can be expressed as follows:

$$P_{loss} = P_{cu} + P_{iron}, \tag{6}$$

where P_{cu} is the stator winding copper losses and P_{iron} is the total stator and rotor iron core losses. For SRG there are no rotor copper losses as there are no windings in the rotor.

The Steinmetz model for the core loss is given by

$$P_{iron} = p_{hys} + P_{eddy}, \tag{7}$$

$$P_{iron} = K_{hys} f^{\alpha} B_m^{\beta} + K_{eddy} (s f B_m)^{(2)}, \tag{8}$$

where B_m represents the flux density at frequency f, P denotes the time-average power loss per unit volume, and K_{hys}, α, β, and K_{eddy} are the loss coefficients referred from Simcenter MAGNET (siemens electromagnetic software) which is given in Table 3.

From equation (8), it can be seen that when the frequency increases the losses increases. Mostly in the urban area, the wind velocity varies from 3 m/s to 6 m/s. For the wind velocity of 3 m/s to 6 m/s, the rotor speed varies from 382 rpm to 764 rpm. The maximum switching frequency of 8/6 SRG and 12/8 SRG is 77 Hz and 102 Hz, respectively, for the wind velocity of 6 m/s.

In this paper, the iron losses are calculated for frequencies of 77 Hz (8/6 SRG) and 102 Hz (12/8 SRG) using equation (8). Figure 3 compares the iron loss curves of the magnetic core material grades chosen for analysis for 8/6 SRG and 12/8 SRG.

From Figure 3, it is observed that even at very high flux densities, the Vacoflux steel has a lower iron loss of 0.3845 W/kg and 0.518 W/kg for 8/6 SRG and 12/8 SRG, making it ideal for high-speed and high-frequency applications. The iron loss in 35C270 steel is 6.7 W/kg and 8.7 W/kg for 8/6 SRG and 12/8 SRG. The iron losses are heat sources that raise the temperature of SRG. Hence, from the iron loss curves of different core materials, it is clear that the

Table 2: Axial length to rotor diameter (L/D_r) ratio.

S. no	Material	L/D_r ratio
I	CR steel	1.026667
II	Hiperco	0.88
III	HyMu	2.173333
IV	35C240	1.093333
V	35C300	1.08
VI	35C360	1
VII	35C530	1.053333
VIII	35C270	1.12
IX	35C330	1.106667
X	Vacoflux	0.886667

Table 3: Material loss coefficient for different core materials.

Material	K	α	β	K
Hiperco	0.0073888	1.15262	1.72219	$5.04373e-005$
HyMu	0.0002021	1.3816	1.88647	$2.05842e-005$
35C240	0.02703	1	1.8308	0
35C300	0.0219365	0.995059	1.72668	$7.42869e-005$
35C360	0.0121491	1.18349	1.84037	$4.74616e-005$
35C530	0.0141494	1.14496	1.81131	$6.20044e-005$
35C270	0.0090129	1.20701	1.77142	$3.24461e-005$
35C330	0.0075437	1.29522	1.79624	$3.11146e-005$
Vacoflux	0.0101653	1.07506	1.48083	$3.8118e-006$

material selection is important to minimize the losses to improve the thermal behavior of the generator and its efficiency.

5. Finite Element Analysis

1 kW SRG used as a standalone wind generator with pole configuration, 8/6 SRG and 12/8 SRG, for a wind velocity of 3 m/s to 6 m/s is designed using the TRV method [2]. The dimensions of the designed generator are given in Table 4. Keeping these dimensions constant, performance analysis has been carried out for various core materials given in Table 1.

5.1. Static Analysis. With phase A, winding excited with rated current and other phases unexcited, the inductance variation and static torque variation for various rotational angles for various core materials are obtained using static analysis. The simulation results of inductance variation for different core materials are shown in Figure 4 for 8/6 SRG and 12/8 SRG.

From Figure 4, the maximum inductance value is 43.7 mH for Hiperco and 17.6 mH for HyMu for 8/6 SRG. The maximum inductance value is 32.8 mH for Hiperco and 13.26 mH for HyMu for 12/8 SRG. For example, comparing the maximum inductance values of 35C360 and Hiperco there is a 21% (8/6 SRG) and 24% (12/8 SRG) increase in inductance value for Hiperco compared to 35C360. The simulation results show that the machine's inductances are influenced by the material properties due to the variation in permeability.

The static torque variation for various rotational angles for various core materials using static analysis is shown in Figure 5 for 8/6 SRG and 12/8 SRG.

From Figure 5, the maximum static torque value is 11.08 Nm for Hiperco and 4.94 Nm for HyMu for 8/6 SRG. The maximum static torque value is 8.34 Nm for Hiperco and 5.04 Nm for HyMu for 12/8 SRG. For example, comparing the maximum static torque values of 35C360 and Hiperco there is a 13% (8/6 SRG) and 7% (12/8 SRG) increase in static torque value for Hiperco compared to 35C360.

5.2. Dynamic Analysis. The generated voltages of 8/6 SRG and 12/8 SRG with different core materials are shown in Figure 6. For each material, generated voltage and ripple vary.

The peak generated voltage for Hiperco is 125 V (8/6 SRG) and 104 V (12/8 SRG). The peak generated voltage for HyMu is 62 V (8/6 SRG) and 54 V (12/8 SRG). Comparing peak generated voltage values of 35C360 and Hiperco there is a 19% (8/6 SRG) and 6% (12/8 SRG) increase in peak generated voltage for Hiperco compared to 35C360.

The iron and ohmic losses of 8/6 SRG and 12/8 SRG for different core materials are shown in Figure 7.

HyMu has low iron and ohmic losses, but output performance is less compared to other core materials. Vacoflux and Hiperco have next lower ohmic losses compared to other core materials. Comparing iron and ohmic losses values of 35C360 and Hiperco there is a 12% (8/6 SRG) and 11% (12/8 SRG) reduction in iron and ohmic losses for Hiperco compared to 35C360.

According to the static and dynamic analysis results shown in Figures 4–7, Vacoflux and Hiperco materials produce higher inductance, generated voltage, and torque, while HyMu produces lower inductance, generated voltage, and torque. Vacoflux and Hiperco core materials have lower iron losses than other materials. Vacoflux has the least H value compared to other core materials. Hence for a higher rating, SRG Vacoflux cannot be used. From the analysis, it is found that Hiperco is the best steel grade which has the highest performance such as low iron loss and ohmic loss, high inductance, and generated voltage among the core materials taken for study followed by 35C360A material. The cost of Hiperco material is almost double the cost of 35C360 material. Considering the cost, 35C360 core material is the next promising core material. In this paper, 35C360 material is used as the core material for the prototypes developed.

6. Thermal Analysis

Thermal steady state analysis was carried out for 1 kW 8/6 SRG and 12/8 SRG with different core materials using the electromagnetics losses got from dynamic analysis. The temperature due to electromagnetic losses of 8/6 SRG and 12/8 SRG with different core materials for rated load from the thermal simulation results are shown in Table 5. The thermal distribution of 8/6 SRG and 12/8 SRG with 35C360 core material is shown in Figure 8.

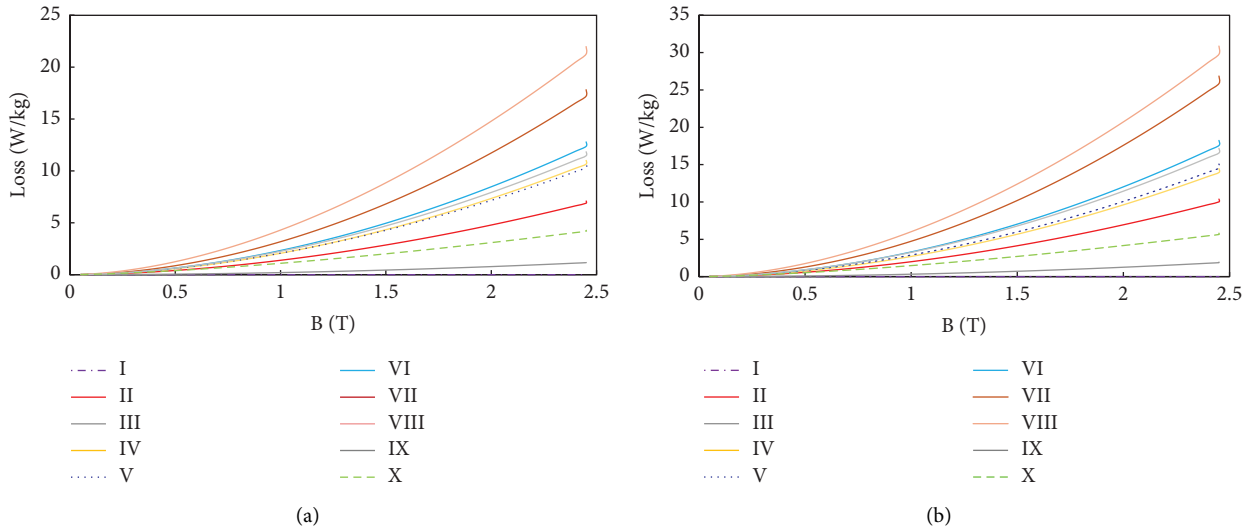

Figure 3: Iron loss curves of magnetic core steels for (a) 8/6 SRG (77 Hz) and (b) 12/8 SRG (102 Hz).

Table 4: Machine dimensions.

Parameters	Machine dimensions	
	12/8	8/6
Stator outer radius (r_O)	75 mm	
Bore radius (r)	37.85 mm	
Air gap (g)	0.35 mm	
Stack length (L)	75 mm	
Rotor outer radius (r_r)	37.5 mm	
Width of stator tooth (W_s)	9.88 mm	13.8 mm
Width of rotor tooth (W_r)	10.4 mm	15 mm
Back-iron thickness of stator (Y_s)	7.45 mm	10.35 mm
Back-iron thickness of rotor (Y_r)	6.8 mm	8.3 mm
Stator pole height (h_s)	29.7 mm	26.8 mm
Rotor pole height (h_r)	10.5 mm	10.5 mm
Number of turns per pole (T_p)	55	100

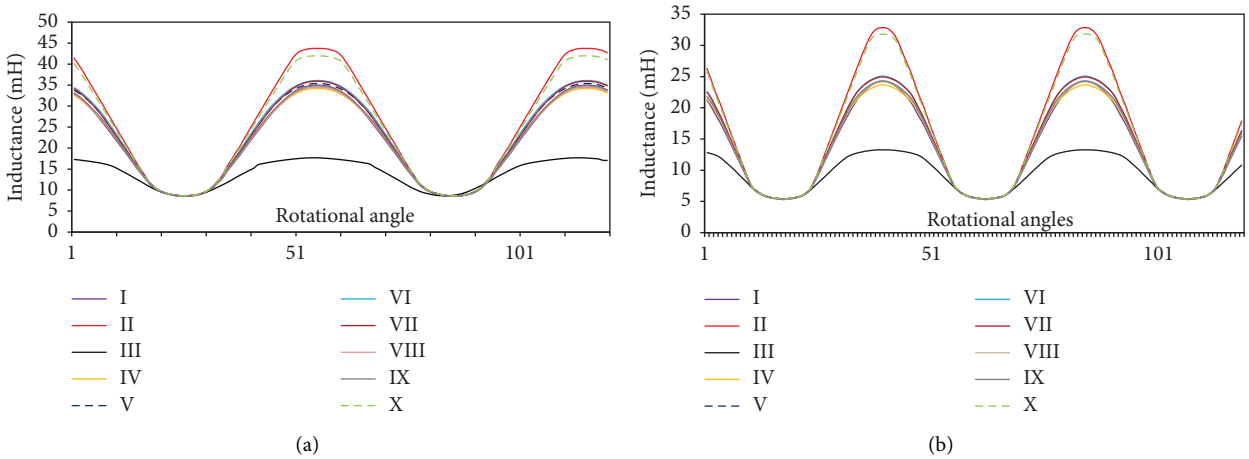

Figure 4: Inductance curves of (a) 8/6 SRG and (b) 12/8 SRG.

The power output of SRG varies with different core materials due to the variation in generated voltage. In Table 5, even though HyMu has the lowest steady-state temperature, the power output is only 464 watts, hence this material is not considered for the study. From the thermal analysis, it has been found that the temperature

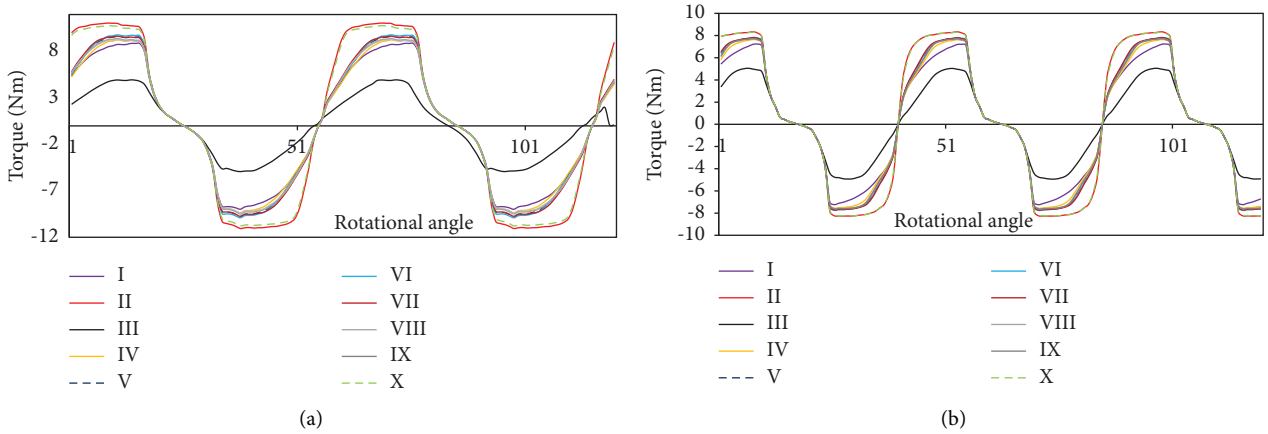

Figure 5: Torque curves of (a) 8/6 SRG and (b) 12/8 SRG.

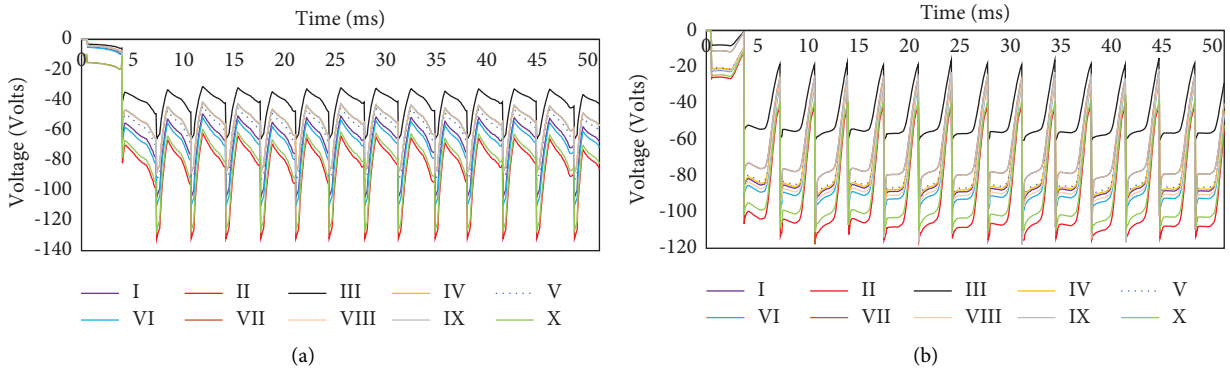

Figure 6: Generated voltages for (a) 8/6 SRG and (b) 12/8 SRG.

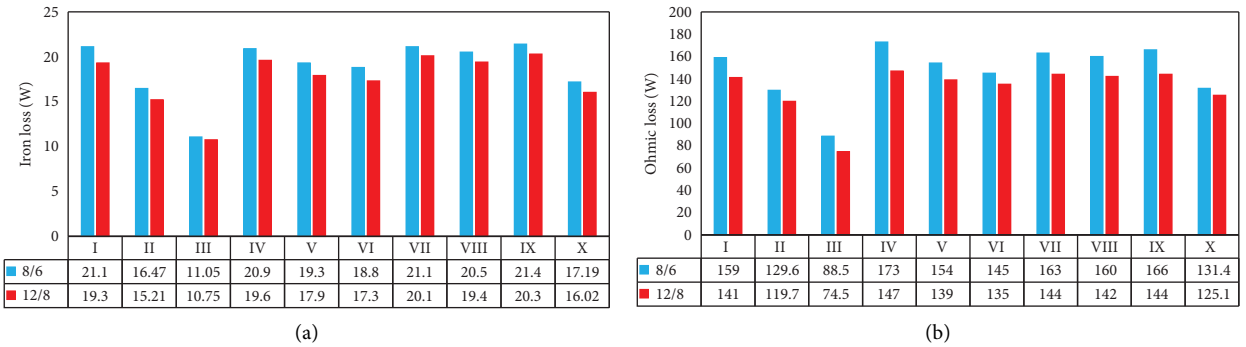

	I	II	III	IV	V	VI	VII	VIII	IX	X
8/6	21.1	16.47	11.05	20.9	19.3	18.8	21.1	20.5	21.4	17.19
12/8	19.3	15.21	10.75	19.6	17.9	17.3	20.1	19.4	20.3	16.02

	I	II	III	IV	V	VI	VII	VIII	IX	X
8/6	159	129.6	88.5	173	154	145	163	160	166	131.4
12/8	141	119.7	74.5	147	139	135	144	142	144	125.1

Figure 7: (a) Ohmic loss and (b) iron loss of 8/6 SRG and 12/8 SRG.

inside SRG using Vacoflux, Hiperco, and 35C360 materials is less compared to other materials. The output power of SRG using Vacoflux, Hiperco, and 35C360 are 1.13 kW, 1.12 kW, and 1 kW, respectively. Considering the cost and easy availability, 35C360 material is chosen as the core material for fabrication.

7. Hardware Results

Prototypes of 1 kW 8/6 SRG and 12/8 SRG are fabricated using 35C360 core material which is shown in Figure 9.

The test setup for inductance measurements for the fabricated SRG is shown in Figure 10. The inductance is

Table 5: Temperature in SRG different core materials for the rated load.

Materials	SRG temperature (°C)					
	Stator core		Rotor core		Stator coil	
	8/6	12/8	8/6	12/8	8/6	12/8
CR steel	72.7	69.9	62.4	59.2	81.4	76.2
Hiperco	65.4	63.8	57.5	55.1	72.4	68.1
HyMu	53.7	53.5	47.4	46.9	58.6	58.9
35C240	76.6	77	65.2	65.4	86.1	86.2
35C300	72.5	73.9	62.8	63.9	81.2	82.3
35C360	69.5	67.7	59.8	56.8	78.4	73.5
35C530	78.1	77.3	67.1	66.8	86.2	84.9
35C270	73.5	70.6	63.4	60	82.6	77.3
35C330	74.6	70.2	63.8	60.4	83.9	80.2
Vacoflux	65.4	61.8	56.5	53.8	72.6	68.4

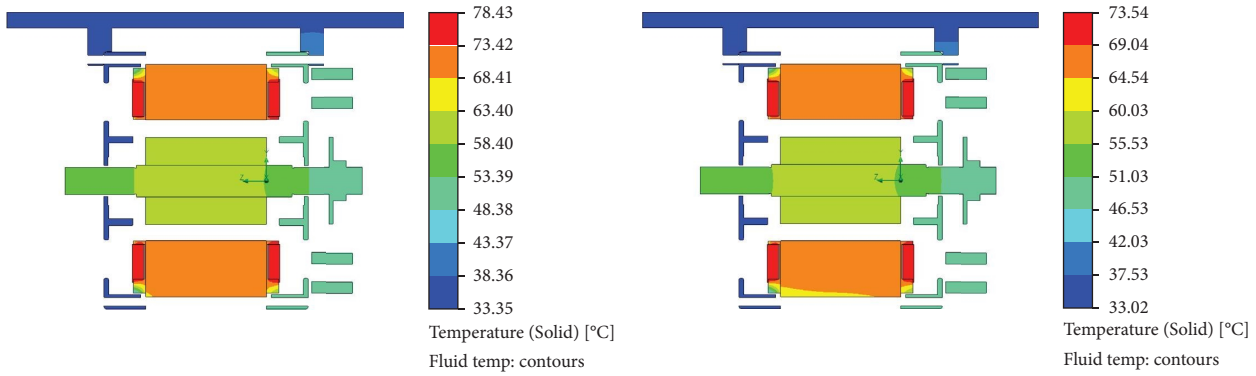

Figure 8: Thermal distribution for (a) 8/6 SRG and (b) 12/8 SRG.

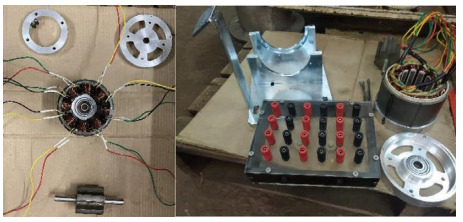

Figure 9: Fabricated 8/6 SRG and 12/8 SRG models.

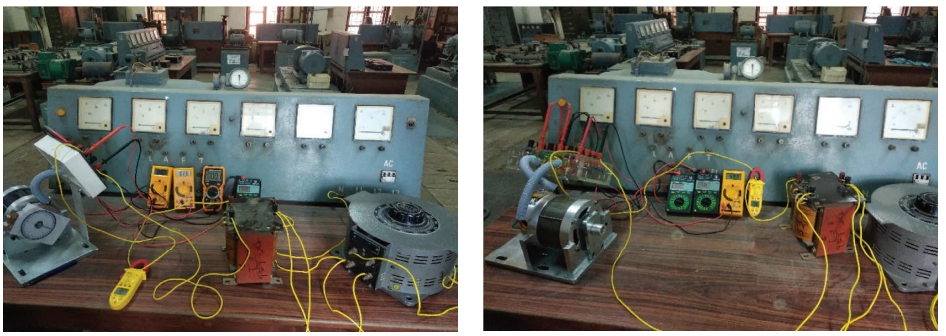

(a) (b)

Figure 10: Experimental test setup for the measurement of inductance of (a) 8/6 SRG and (b) 12/8 SRG.

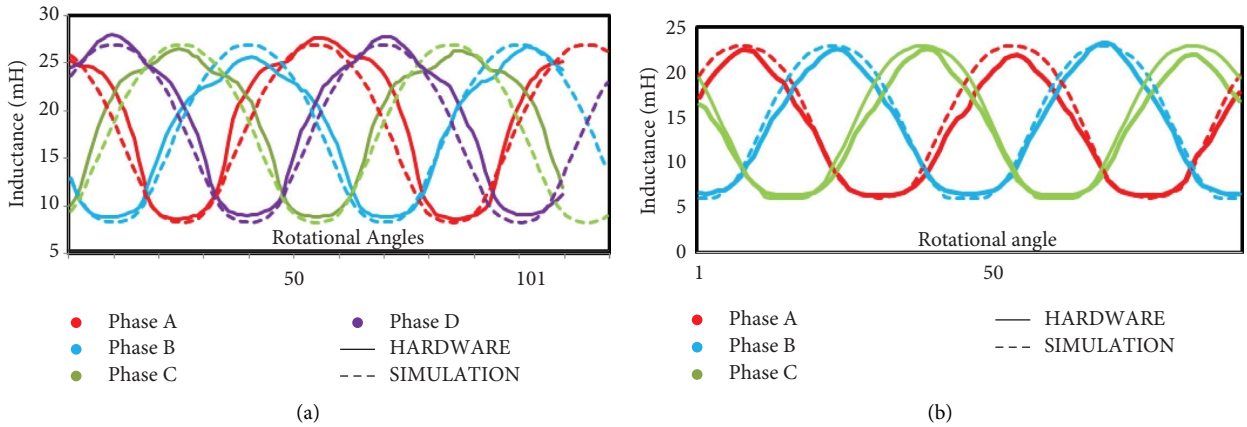

Figure 11: Inductance profile for (a) 8/6 SRG and (b) 12/8 SRG.

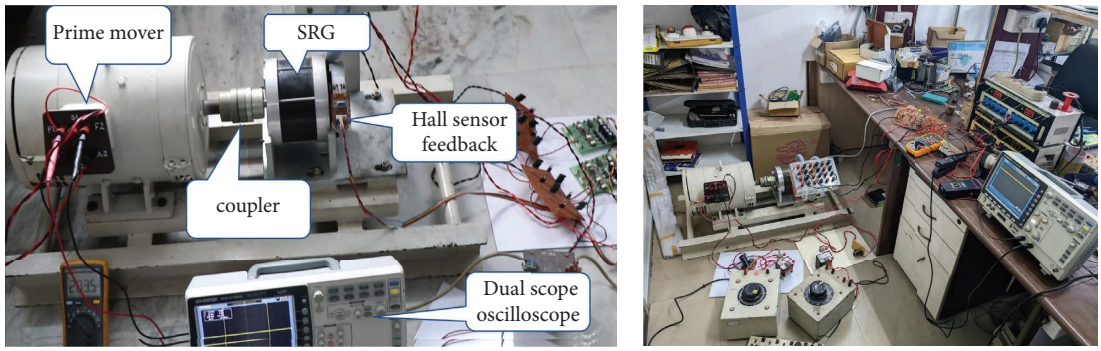

Figure 12: Experimentation setup for generated voltage measurement of (a) 8/6 SRG and (b) 12/8 SRG.

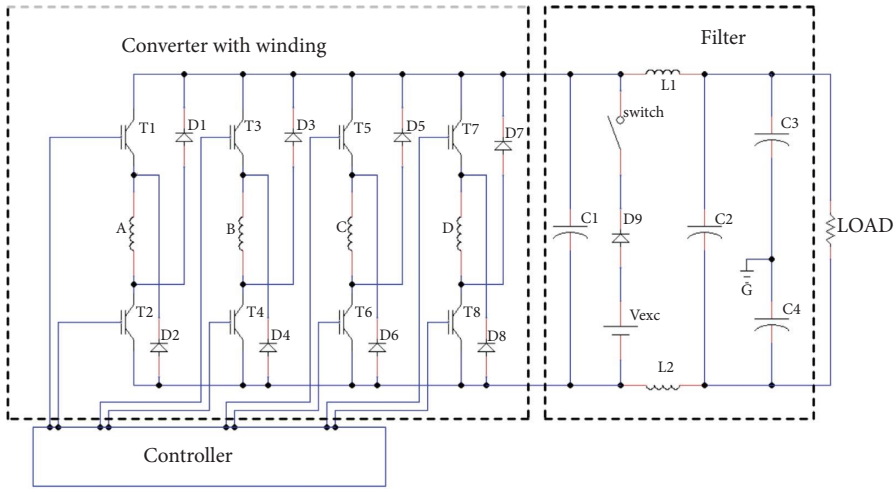

Figure 13: Circuit diagram of SRG interfaced with converter and filter.

measured for various rotational angles for 8/6 SRG and 12/8 SRG.

Figure 11 shows the inductance variation for various rotational angles by simulation and experimentation. Experimentation results match with simulation results with less than 5% error.

Figure 12 shows the experimental setup for SRG-generated voltage measurement.

Figure 13 shows the circuit diagram of the SRG interface with an asymmetric converter and filter circuit. The initial excitation is given by the DC source (V_{exc}). DC motor is coupled to the SRG shaft. DC motor acts as a wind emulator.

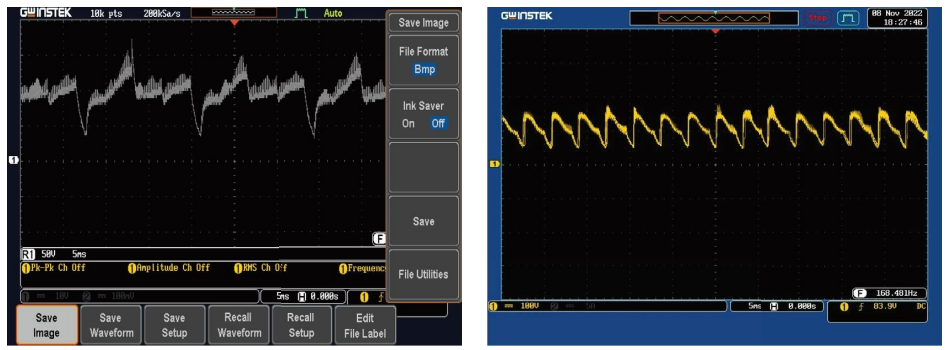

(a) (b)

Figure 14: Generated voltage without filter circuit for (a) 8/6 SRG and (b) 12/8 SRG with 764.

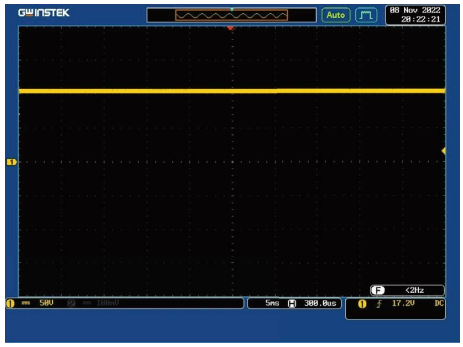

Figure 15: Generated voltage with filter circuit.

Table 6: Generated voltage with different RPM.

Speed (RPM)	Voltage (volt)	
	8/6 SRG	12/8 SRG
764	96.1	96.1
700	95.9	95.9
650	95.7	95.9
550	95.5	95.8
450	95.3	95.7
400	95.2	95.6
360	95.1	95.6

The speed of the DC motor is varied from 360 rpm to 764 rpm corresponding to windspeed of 3 m/s to 6 m/s. Figure 14 shows the generated voltage for 8/6 SRG and 12/8 SRG without a filter circuit. Figure 15 shows the generated voltage with the filter circuit. Table 6 gives the generated voltage for various speeds. From Figures 13 and 14, it is found that the generated voltage of 8/6 SRG has more ripple with low frequency whereas 12/8 SRG has a lower voltage ripple with high frequency.

8. Conclusions

This paper has analyzed the effect of magnetic core material on sizing and the performance of SRG used in wind energy systems. In this study, ten different magnetic core materials with 0.35 mm thickness grades are considered. Keeping the power output constant, it has been found that the power density of SRG increased with an increase in flux density (B_m), using different core materials. Keeping the dimensions constant, a performance comparison of SRG using various core materials in terms of inductance, generated voltage, iron loss, ohmic loss, and torque has been carried out using static, transient, and thermal analysis. From the analysis, it is found that Hiperco is the best core material which has the highest performance among the core materials taken for the study. Due to the cost, the next promising material 35C360 core material is used for the fabrication of prototypes of 1 kW 8/6 SRG and 12/8 SRG. Experimentation results of the inductance, losses, and output voltage variation for various rotational angles of the fabricated SRG matched with simulation results with less than 5% error. The generated voltage of 12/8 SRG has a lower voltage ripple compared to 8/6 SRG. From the analysis, it is concluded that the core material selection is important to develop an SRG with increased power density, generated voltage, torque, higher efficiency with reduced losses, and good thermal behavior. The design tradeoff for selecting core material for SRG are BH curve with less iron loss, material availability, and cost. From this detailed analysis, 12/8 SRG is best suited for a 1 kW wind generator.

Data Availability

No underlying data were collected or produced in this study.

Conflicts of Interest

The authors declare that they have no conflicts of interest.

Acknowledgments

The authors would like to thank the Council of Scientific and Industrial Research (CSIR-HRDG) (File no.: 09/468/0514/2018EMRI-I), Government of India, for their support.

References

[1] M. Z. Lu, P. H. Jhou, and C. M. Liaw, "Wind switched-reluctance generator based microgrid with integrated plug-in energy support mechanism," *IEEE Transactions on Power Electronics*, vol. 36, no. 5, pp. 5496–5511, 2021.

[2] T. J. E. Miller, *Switched Reluctance Motors and Their Control*, Magna, Oxford, OH, USA, 1993.
[3] R. Krishnan, *Switched Reluctance Machine Drives: Modeling, Simulation, Analysis, Design, and Applications*, Taylor & Francis, Boca Raton, FL, USA, 2001.
[4] Y. Sugawara and A. Kan, "Characteristics of a switched reluctance motor using grain-oriented electric steel sheet," in *Proceedings of the 2013 IEEE ECCE Asia Downunder*, pp. 26–29, ICEMS, Melbourne, Australia, June 2013.
[5] M. A. Prabhu, J. Y. Loh, S. C. Joshi et al., "Magnetic loading of soft magnetic material selection implications for embedded machines in more electric engines," *IEEE Transactions on Magnetics*, vol. 52, no. 5, pp. 1–6, 2016.
[6] M. F. Ashby, H. Shercliff, and D. Cebon, *Materials: Engineering, Science, Processing and Design*, Butterworth-Heinemann, Oxford, UK, 2nd edition, 2009.
[7] M. Rippy, "An overview guide for the selection of lamination materials," *Motion*, vol. 8, 2015.
[8] F. Bloch, T. Waeckerle, and H. Fraisse, "The use of iron-nickel and iron-cobalt alloys in electrical engineering, and especially for electrical motors," in *Proceedings of the 2007 Electrical Insulation Conference and Electrical Manufacturing Expo*, Nashville, TN, USA, October 2007.
[9] Y. Nakazawa, K. Ohyama, K. Nouzuka, H. Fujii, H. Uehara, and Y. Hyakutake, "Design method for improving motor efficiency of switched reluctance motor," *Electrical Engineering in Japan*, vol. 195, no. 1, pp. 40–52, 2016.
[10] A. Krings and J. Soulard, "Overview and comparison of iron loss models for electrical machines," *Journal of Electrical Engineering*, vol. 10, p. 162, 2010.
[11] M. A. Raj and A. Kavitha, "Impact of magnetic core steel grade on the performance of synchronous reluctance motor with transversally laminated anisotropic (TLA) rotor core for e-auto rickshaw application," *Journal of Magnetics*, vol. 25, no. 4, pp. 503–510, 2020.
[12] N. Bianchi, M. Degano, and E. Fornasiero, "Sensitivity analysis of torque ripple reduction of synchronous reluctance and interior PM motors," *IEEE Transactions on Industry Applications*, vol. 51, no. 1, pp. 187–195, 2015.
[13] S. Taghavi and P. Pillay, "A sizing methodology of the synchronous reluctance motor for traction applications," *IEEE Journal of Emerging and Selected Topics in Power Electronics*, vol. 2, pp. 329–340, 2014.
[14] J. Fang and S. Xu, "Effects of eddy current in electrical connection surface of laminated cores on high-speed PM motor supported by active magnetic bearings," *IEEE Transactions on Magnetics*, vol. 51, no. 11, pp. 1–4, 2015.
[15] J. Kartigeyan and M. Ramaswamy, "Effect of material properties on core loss in switched reluctance motor using non-oriented electrical steels," *Journal of Magnetics*, vol. 22, no. 1, pp. 93–99, 2017.
[16] M. Ramkumar and K. Latha, "Selection of pole numbers for a 1 kW switched reluctance generator for wind energy conversion by electromagnetic considerations," in *Proceedings of the 2019 IEEE 1st International Conference on Energy, Systems and Information Processing (ICESIP)*, pp. 978–981, IEEE-ICSIP, Chennai, India, July 2019.